Final Technical Report (FTR)

Cover Page

a. *Federal Agency*	Department of Energy	
b. *Award Number*	DE-EE0009369	
c. *Project Title*	Development of organic-inorganic hybrid selective layers via vapor phase infiltration to enhance the durability of perovskite solar cells	
d. *Recipient Organization*	Georgia Tech Research Corporation	
e. *Project Period*[1]	*Start: 05/01/2021*	*End: 10/31/2022*
f. *Budget Period*	*Start: 05/01/2021*	*End: 10/31/2022*
g. *Reporting Period*	*Start: 05/01/2021*	*End: 10/31/2022*
h. *Report Term or Frequency*	Quarterly	
i. *Principal Investigator (PI)*	Juan-Pablo Correa-Baena Assistant Professor jpcorrea@gatech.edu 404-894-2197	
j. *Business Contact (BC)*	Christopher D'Urbano Manager for Grants and Contracts Administration E-mail: ced@gatech.edu Phone: 404-313-1735	
k. *Certifying Official (if different from the PI or BC)*	//	

_____ _____

Signature of Certifying Official *Date*

By signing this report, I certify to the best of my knowledge and belief that the report is true, complete, and accurate. I am aware that any false, fictitious, or fraudulent information, misrepresentations, half-truths, or the omission of any material fact, may subject me to criminal, civil or administrative penalties for fraud, false statements, false claims or otherwise. (U.S. Code Title 18, Section 1001, Section 287 and Title 31, Sections 3729-3730). I further understand and agree that the information contained in this report are material to Federal agency's funding decisions and I have any ongoing responsibility to promptly update the report within the time frames stated in the terms and conditions of the above referenced Award, to ensure that my responses remain accurate and complete.

[1] *If you have received No Cost Time Extensions (NCTE), please add a note below the table indicating the length of each one and which budget periods were affected.*

1. **Acknowledgement:** "This material is based upon work supported by the U.S. Department of Energy's Office of Energy Efficiency and Renewable Energy (EERE) under the Solar Energy Technologies Office FOA DE-TA8-0002243 Award Number DE-EE0009369."

2.

3. **Executive Summary:** Despite the rapid increase in power conversion efficiency (PCE) of perovskite solar cells (PSCs) over the last decade, stability remains a major roadblock to commercialization. This work proposes the use of vapor phase infiltration (VPI) as a tool to create hybrid organic-inorganic layers that improve the stability of organic charge transport layers, such as hole-selective spiro-OMeTAD in these PSC and other organic electronic devices. Using X-ray photoelectron spectroscopy (XPS), ultraviolet photoelectron spectroscopy (UPS), and grazing incident wide-angle X-ray scattering (GIWAXS), we identify that infiltration of TiO_X via VPI hinders the crystallization of the spiro-OMeTAD layer by likely preventing the π- π stacking of the molecules. Infiltrated PSCs retained around 80% of their original efficiency after an *operando* stability test of 60 h at 75 °C, double the efficiency retained by devices without infiltration. This work provides a blueprint for using VPI to stabilize organic charge transport layers via prevention of π- π stacking that leads to deleterious crystallization that shortens device lifetimes.

Two solar companies with active research on metal halide perovskites and with expertise on vapor deposition processes have been contacted and agreed to an interview in-person to provide feedback on the technology developed. Both companies demonstrated interest in a process able to enhance the thermal stability of the hole selective layers. Cost of materials was not identified as a risk for industrial implementation, as most of the cost is imbedded in the glass, with the active layers being marginal costs. However, the time required for post-treatment to stabilize the interface was pointed as a potential risk to implementation. The specific choice of spiro-OMeTAD as interlayer to be stabilized was not seen as a risk at least one of the companies we interviewed.

This SETO funding has provided a new approach to stabilize PSCs when tested at high temperatures. These results are important to provide the USA leadership in producing low-cost, high efficiency and stable solar cells that can have significant

impact on LCOE. LCOE critically depends on long term durability, and at the current reliability prospects, it will be difficult to achieve LCOE lower than 25 ¢/kWh.

4. Table of Contents:

5. Background: Metal halide perovskite solar cells (PSCs) have shown enormous potential to lower the cost of solar energy[1]. In just a decade, their power conversion efficiency (PCE) has rapidly increased to over 25% [2–4], surpassing other technologies, such as CIGS and CdTe, while employing readily available elements. However, long-term stability remains the major barrier to their commercialization. The perovskite layers, especially those containing methylammonium (MA), are susceptible to degradation when exposed to moist air and high temperatures.[5]. Studies have shown that alloying MA with Cs- and formamidinium (FA) can improve the thermal stability of the perovskite layer[6]. Cs and FA alloying also allows for tuning the crystallographic structural phase, which ultimately dictates long-term stability[7]. While the perovskite layer has been of concern due to these degradation mechanisms, the charge transport layers have been identified as main causes of degradation in a PSC. The most commonly used electron transport layer is TiO_2, which absorbs UV light and initiates a photocatalytic degradation of the perovskite layer[8,9]. Traditional hole transport layers (HTL) are thin films of small molecules, such as 2,2',7,7'-Tetrakis[N,N-di(4-methoxyphenyl)amino]-9,9'-spirobifluorene (spiro-OMeTAD). Spiro-OMeTAD enables efficient hole collection, which resulted in most of published world record efficiencies[3,4], but it suffers from poor long term stability[10–12].

There are three main degradation pathways for spiro-OMeTAD during solar cell operation. The first is caused by dopants. Spiro-OMeTAD requires the use of dopant additives to improve its conductivity through the formation of oxidized spiro$[TFSI]_2$[13,14]. Although this is beneficial for the initial performance of the devices, spiro$[TFSI]_2$ rapidly reacts with iodide ions that migrate from the perovskite layer and reduces back to spiro-OMeTAD, which decreases the conductivity of the layer over time[13]. In the second pathway, the spiro-OMeTAD layer allows the migration of gold ions from the back contact into the perovskite layer, which has been suggested as another route to irreversible degradation of PSCs[15]. The third degradation pathway for this charge transport layer involves the crystallization of spiro-OMeTAD at temperatures as low as 65 °C[16]. Studies have shown that degradation of the spiro-OMeTAD layer happens at temperatures where the bulk of the perovskite layer is not significantly degraded[17–19]. While the perovskite layer can withstand temperatures up to 120 °C without showing signs of degradation in X-ray diffraction (XRD) or ultraviolet-visible (UV-VIS) absorption spectroscopy, the hole mobility of the spiro-OMeTAD layer decreases when devices are subject to several heating cycles at 70 °C[20]. Further, formation of

cracks and delamination has also been observed on spiro-OMeTAD layers under operation when stressed to 75 °C[16].

Efforts to combat the stability issues of halide perovskite absorbers have focused on changes to selective contact layers from organics to metal oxides.[21,22] The latter approach has been implemented because most organics crystalize at low temperatures (50-100 ºC) leading to cracking and delamination of the thin films and thus to rapid degradation of the device [23–25]. Recent work has demonstrated that an amorphous TiO_2 layer deposited by atomic layer deposition (ALD) between the spiro-OMeTAD layer and Au electrodes can improve the performance of perovskite solar cells and prevent diffusion of ions in between layers[26]. ALD is well known to be an effective deposition method to grow conformal, pinhole-free thin films to provide stability by encapsulation[27–30] and has been studied for other PSC applications[31–33]. However, most metal oxide thin films do not have well aligned band edges with the HTLs, which can lead to low charge carrier extraction efficiencies, motivating the search for a hybrid approach where the metal oxide is not blocking extraction of carriers.

Vapor phase infiltration (VPI) is a deposition technique related to ALD that has been used to form organic-inorganic hybrid materials with unique properties[34,35]. In contrast to ALD, VPI infuses the gaseous precursors into the subsurface of polymeric materials, leading to chemical reactions with the polymer that form inorganic metal oxide clusters within the polymer. Thus, unlike ALD that forms a coating on the surface, VPI modifies the bulk chemistry of the polymer, forming a new organic-inorganic hybrid material[36], enabling improved chemical stability[37,38] and modified thermal properties[39]. During the VPI process, a solid polymer or small molecule substrate is exposed to a metal containing precursor (e.g. metalorganics, metal halides) in the vapor phase. Depending upon precursor chemistry, substrate chemistry, and VPI processing parameters, the precursor will sorb within the film, diffuse, and become entrapped. Entrapment occurs either via chemical interaction with the substrate or by reaction with a co-reactant subsequently introduced, leading to a nonvolatile material (often a metal oxide cluster of just a few atoms).

In this study, we infiltrate spiro-OMeTAD thin films with TiOx clusters to improve the device stability while not compromising solar cell efficiency. Using X-ray photoelectron spectroscopy (XPS) depth profiling, TiO_X is found to infiltrate about 30-40 nm into the spiro-OMeTAD layer. No significant chemical changes are observed in FTIR and XPS, indicating there is no direct chemical bonding between the spiro-OMeTAD and the infiltrated TiOx clusters. We show that the long-term stability of the PSCs is greatly improved by infiltrating TiO_X into the spiro-OMeTAD films. According to GIWAXS measurements, this improvement in long-term stability appears to be related to the TiO_x clusters disrupting the π- π stacking of the spiro-OMeTAD and hindering its crystallization.

6. **Project Objectives:** Describe the impact this project will have on achieving national goals of clean energy progression and economic benefit to the U.S. Describe the project goals, expected outcomes, and significance, innovation, and fundamental advances of the proposed body of work and how they support the claimed impacts. Please include a summary of the tasks within the Statement of Project Objectives

(SOPO) or Technical Work Plan (TWP) for the entire project, including the milestones and go/no-go decision points.
This project aims to develop hybrid organic inorganic thin films as electron selective layers (ESLs) using vapor phase infiltration (VPI) of metal oxide clusters into small molecule conductive layers (e.g., Spiro-OMeTAD). The incorporation of metal oxide cluster into the organic layers will lead to more robust films by inhibiting crystallization and preventing moisture degradation of perovskite solar cells. This SETO funding has provided a new approach to stabilize PSCs when tested at high temperatures. These results are important to provide the USA leadership in producing low-cost, high efficiency and stable solar cells that can have significant impact on LCOE. LCOE critically depends on long term durability, and at the current reliability prospects, it will be difficult to achieve LCOE lower than 25 ¢/kWh.
Here is the list of tasks completed during the project:

a. Task 1.0 – Reference device with average 20% efficiency
b. Task 2.0 – Testing Infiltration of the metal oxide into the ETL
c. Task 3.0 – Incorporate infiltrated HTLs (hole transport layers) into a solar cell stack
d. Task 4.0 – Stakeholder Engagement
e. End of Project (EOP) Goal: Improved thermal stability of perovskite solar cells

7. Project Results and Discussion:

a. Task Number and Title: Task 1.0 – Reference device with average 20% efficiency

Milestone 1.1.1 - 20% Average efficiency for reference device

Milestone 1.1.2 – T95 500 hours at 25°C and nitrogen environment for reference devices

The reference device has an n-i-p architecture where TiO_2 is used as the electron transport material and spiro-OMeTAD as the hole transport material. The device stack is composed by 'Glass | FTO (fluorine doped tin oxide) | compact-TiO_2 | mesoporous- TiO_2 | Perovskite | spiro-OMeTAD | Au', which was selected as starting point for the optimization based on literature reports of the highest efficiencies perovskite solar cells and on previous experiments in the group. The device layout and structure are reported in **Figure 1A and 1B**. Three independent substrates, with 8 solar cells (pixels) per substrate were fabricated for each variation considered in the following experiments to ensure result reproducibility. All device performances were measured using a 3A Litos Lite solar simulator setup from Fluxim. Current-Voltage (J-V) scans were acquired in forward and reverse direction (negative to positive bias and vice versa) in light and dark, to evaluate hysteresis of the devices, the performance meters limiting power conversion efficiency (PCE), as well as the shunt and series resistances introduced by the layers. **Figure 1C** shows the steady-state PCE of the devices measured by following the maximum power point (MPP) for 2 min. **Figure 1D-1G** show the individual performance parameters (short circuit current (Jsc), open circuit voltage (Voc), fill factor (FF) and PCE) taken from the reverse scans. Using a perovskite layer with composition

$Cs_{0.09}FA_{0.91}PbI_3$ passivated on the top and bottom with a solution of 1mg/mL of PEAI in ethanol allows for the highest efficiency. **Figure 1H** shows the stability measurement taken on devices made with a $Cs_{0.17}FA_{0.83}PbI_3$ perovskite layer. It retained 94% of the original efficiency after 500h of measuring the MPP at 1 sun at 25 °C under constant N_2 flow.

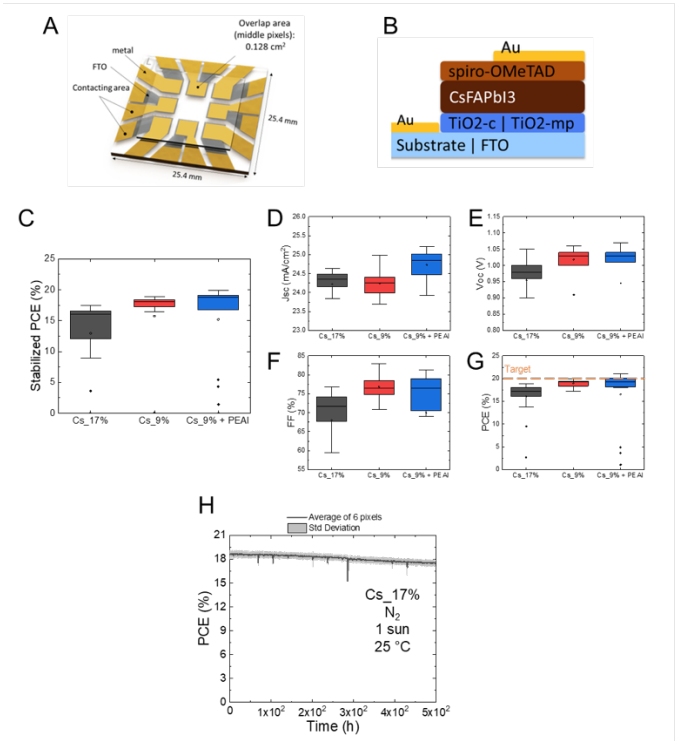

Figure 1 | Device configuration, device performance, and stability. (A) FTO and metal electrode pattern defining 8 individual solar cells on each substrate processed (~0.128 cm^2 unmasked area). (B) Typical layer stack used for device fabrication. (C) Stabilized power conversion efficiencies evolution of reference solar cells. Cs_17% = $Cs_{0.17}FA_{0.83}PbI_3$. Cs_9% = $Cs_{0.09}FA_{0.91}PbI_3$. Cs_9% + PEAI = $Cs_{0.09}FA_{0.91}PbI_3$ + a top and bottom layer of PEAI to passivate the interphases of the perovskite film. (D-G) Individual performance parameter of reference solar cells with changes in the perovskite layer. (H) Stability measurement of reference solar cell made with Cs_17% perovskite.

Additional stability measurements on optimized reference devices were not performed due to the failure of the in-situ MPPT stability setup. Supply chain issues delayed the repairment, and the setup is still at the producer headquarters in Europe. Alternative stability measurements at high temperature were explored as discussed below. The results of representative batches attempted to improve the efficiency of the solar cell devices are presented in **Figure 2** for MACl addition, annealing time optimization of the perovskite layer, and compositional optimization. In all cases no improvements in PCE with respect to the reference were observed.

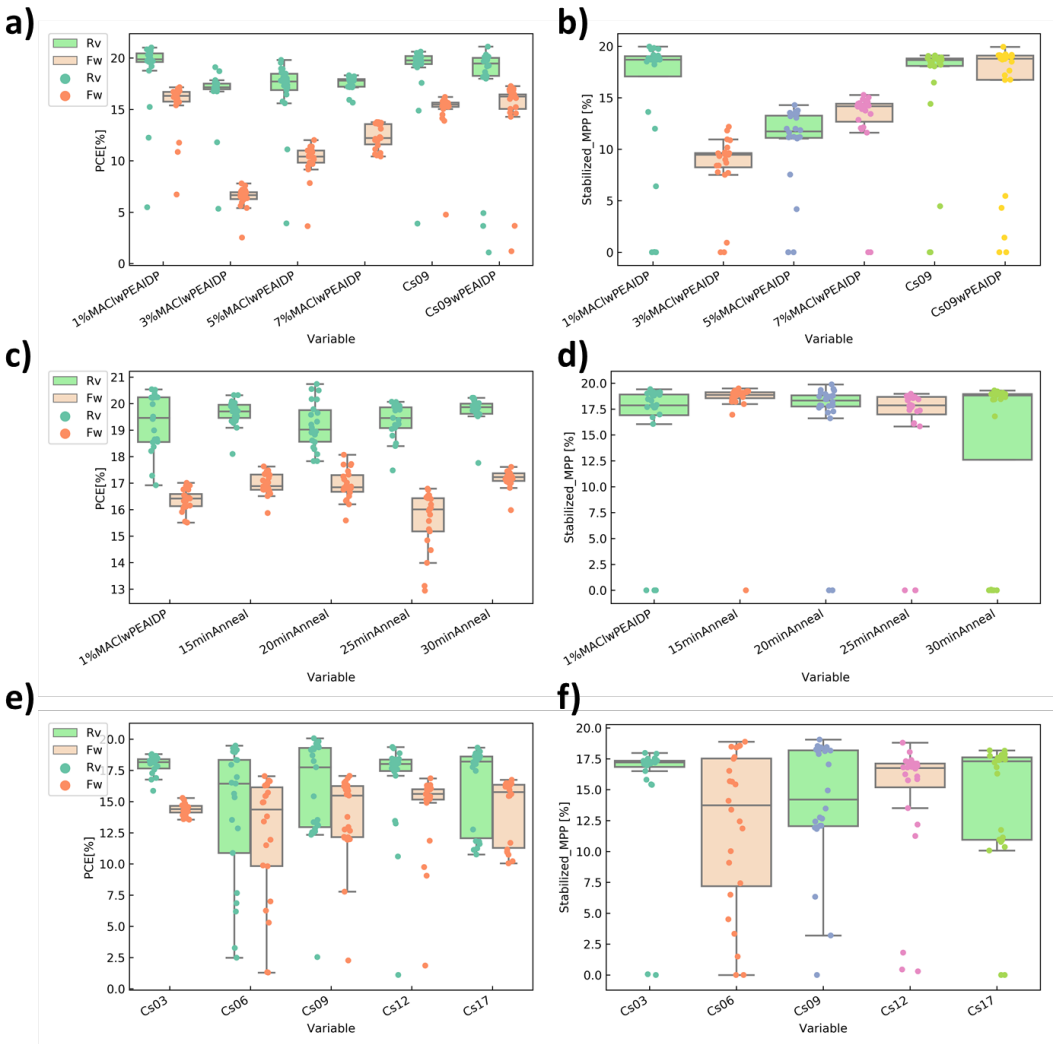

Figure 2 | Different approaches towards reference device performance improvement. (A,C,E) PCE from reverse and forward scans and (B,D,F) PCE stabilized after 1 minute of maximum power point tracking for: devices with different MACl addition in the perovskite precursor solution (A,B); extended annealing time of the $Cs_{0.9}FA_{0.91}PbI_3$ layer (C,D); and different Cs, FA ratios $Cs_xFA_{1-x}PbI_3$.

Planned vs. Actual Activities: It was planned to reach this power conversion efficiency in the first 3 months of the project, but problems with the p-i-n structure caused a delay in the progress of the project. To bypass efficiency limitations the focus has been changed to n-i-p devices. The power conversion efficiency (PCE) of the reference devices was rapidly increased to approach the target. We made several changes to the original perovskite layer to obtain a maximum power conversion efficiency of 21.11% with median value of 19.48% in reversed scans of the JV curve. Additional strategies to further increase the efficiency of the reference devices were pursued, such as the addition of MACl (Methylammonium chloride) to the precursor solution, longer annealing time of the perovskite layer, and bandgap optimization, but no

improvements in the average PCE were observed. The task is considered complete.

Explanation of Variance: Reference solar cells are 0.52% below the target average PCE (20%). Alternative routes to enhance efficiency were attempted, including MACl addition in the perovskite precursor solution, optimization of the annealing time, and exploration of more perovskite compositions. However, no improvement in the average efficiency was detected. Further improvement in efficiency would likely entail a change in the electron transporting layer (ETL). Efforts to develop a SnO_2-based ETL are being pursued, however the effort to further enhance this interface extends beyond the purpose of this work.

b. Task Number and Title: Task 2.0 – Testing Infiltration of the metal oxide into the ETL

Milestone 1.2.1 – Elemental detection of metal infiltration into the spiro-OMeTAD layer

The effect of different parameters such as temperature (70 °C - 90 °C) and exposure time of the precursor gas (5 min to 10 hours) were studied. Preliminary results on the VPI show that running the process at 70 °C allows for infiltration into the spiro-OMeTAD layer without causing significant damage to the device stack. **Figure 3** compares the XPS depth profile elemental spectra for a reference device stack and devices with 3h and 10 h $TiCl_4$ exposure at 70 °C. The Ti2p signal is visible within the first tens of nanometers of the spiro-OMeTAD layer, which is distinguished by the high signal of C1s.

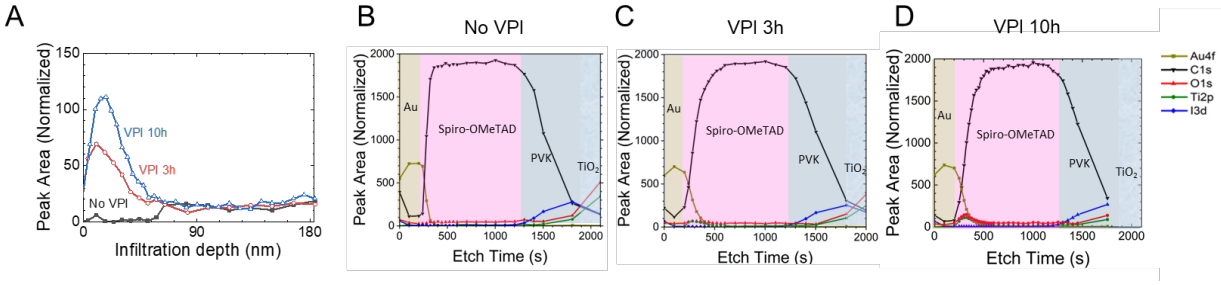

Figure 3 | Infiltration of organic layer. (A) Ti 2p signal on the spiro-OMeTAD layer extracted from the XPS depth profiling for (B) reference solar cell device, (C) 3 h TiO_x infiltrated-spiro-OMeTAD solar cell device, and (D) 10 h TiO_x infiltrated-spiro-OMeTAD solar cell device

Milestone 1.2.2 - Charge carrier mobility of hybrid layer

We attempted a measurement of the mobility of VPI-treated spiro-OMeTAD films deposited on a thin layer of TiO_2 on Si/SiO_2. The thin TiO_2 film was introduced to enhance the wettability of the spiro-OMeTAD film on the Si substrate. **Figure 4** compares spiro-OMeTAD layers obtained on a clean silicon wafer versus a silicon wafer treated with one cycle of spray pyrolysis of TiO_2, showing how this thin layer enhances the wettability of the spiro-OMeTAD film.

Measuring the charge carrier mobility of the spiro-OMeTAD layer was difficult due to the inherent high resistivity of the layer. A conventional 4-probe measurement set-up is not capable of measuring the low currents that flow in this material, and the size of the probes prevents reducing the distance between them. To solve this problem, we used a Keithley 4200 SCS semiconductor analyzer which allows to decrease the distance between the probing points to 20 μm. An Au grid used for transmission electron microscopy was exploited to deposit patterned Au on the substrate with fixed spacing, as shown in the optical microscope image in **Figure 4C**. We processed samples in the architecture 'Si/SiO_2/TiO_2/spiro-OMeTAD/Au' and measured the resistance of the spiro-OMeTAD film by contacting neighboring Au pads disposed in a line. The measurement did not provide reliable estimates of resistance, with values changing of orders of magnitude depending on the bias applied.

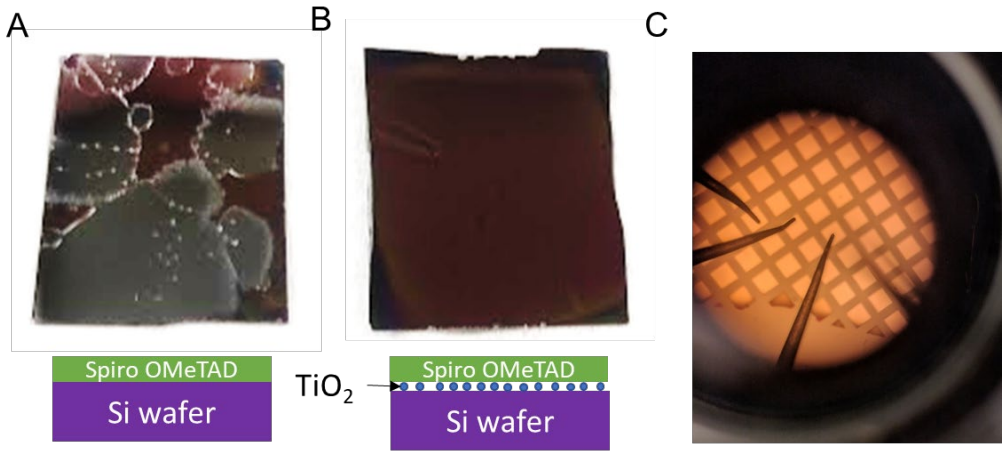

Figure 4 | Coverage of spiro-OMeTAD and 4-probe measurements. (A) On a clean silicon wafer. (B) On a silicon wafer with the deposition of TiO_2 by spray pyrolysis. (C) Resistivity measurement in Keithley 4200 SCS semiconductor analyzer

As an alternative to measure the resistivity of the spiro-OMeTAD layer, we compared the J-V characteristic of complete solar cells. The series resistance can be extracted from the slope of the J-V curve nearby Voc: it is proportional to the reciprocal of the slope of the tangent line in that point. **Figure 5** compares the series resistance extracted from J-V scans taken in forward (FW) and reverse (RV) bias, showing that the series resistance doesn't change significantly for infiltration time up to 10 h.

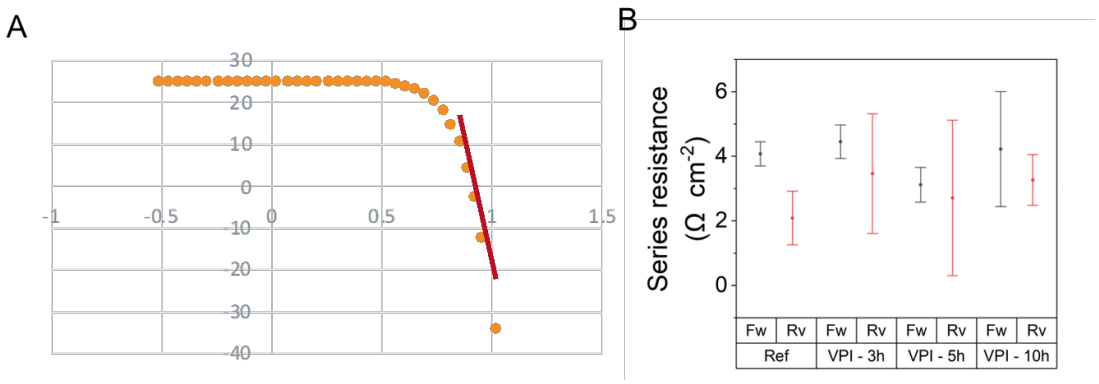

Figure 5 | Series resistance of solar cells. (A) Example of a J-V curve and tangent line to the Voc. (B) Series resistance of solar cells containing spiro-OMeTAD infiltrated with varying exposure times.

Milestone 1.3.2 – Hydrophobicity

Hydrophobicity was assessed by contact angle measurements using a 6mL droplet of water. We found that the overall hydrophobicity of spiro-OMeTAD samples after infiltration decreases compared to the reference. This decrease is related to the presence of -OH groups at the surface as consequence of the formation of the hybrid TiOx:spiro-OMeTAD layer, similarly to what has been observed on different oxides in literature (Nakamura, 2002). Table 1 summarizes the results of the measurements.

Table 1. Water contact angle measurements.

VPI Condition – Spiro-OMeTAD/Si	**Contact Angle**
Undoped Reference	67.88 ± 1.99
Doped Reference	45.63 ± 1.36
3hr $TiCl_4$	33.00 ± 0.56
5hr $TiCl_4$	26.50 ± 0.77
10hr $TiCl_4$	38.90 ± 0.35

Milestone 1.3.1 – Glass transition measurement

We implemented a method to obtain the glass transition temperature from the thickness of the thin film measured with ellipsometry at different temperatures. We extracted the glass transition temperature (T_g) by monitoring the change in thermal expansion coefficient of the sample (where the slope of thickness vs temperature curve changes). We performed the measurement on the stack

'Si/SiO_2/TiO_2/spiro-OMeTAD'. **Figure 6A,B** show that the thermal expansion coefficient of pristine spiro-OMeTAD changes at ~100 °C, while for infiltrated sample for 10 h at 70 °C, the change is at ~90 °C. The T_g increases slightly for thinner films but it remains lower in the VPI-treated samples. This means that the VPI treatment decreases the T_g of spiro-OMeTAD. The thinner films were also measured to allow us to have a more representative descriptor of the infiltrated part of the spiro-OMeTAD film. Trends of the decrease as a function of infiltration time and spiro-OMeTAD film thickness are presented in **Figure 6C**. The decrease in Tg could be related to a disruption of the pi-pi interactions of the aromatic rings in spiro with the VPI process, which would make the spiro-OMeTAD molecules more mobile. XPS supported this hypothesis as the intensity of the π-π* satellite peak decreases with longer VPI exposure times**.** **Figure 7** present the XPS surface scans of infiltrated spiro-OMeTAD with varying exposure times.

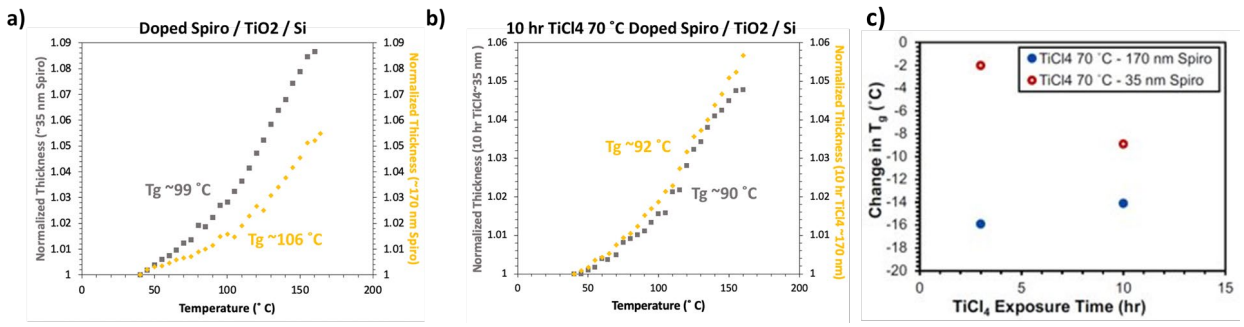

Figure 6 | Glass transition temperature. Glass transition temperature calculation from thickness Vs temperature curves obtained with ellipsometry. A pristine spiro film is presented in (A) with two different thicknesses (~35 nm, ~170 nm). A VPI-treated spiro film is presented in (B) treated for 10 h at 70 °C. (C) shows the change in Tg with respect to the reference for films of different thicknesses infiltrated for different times.

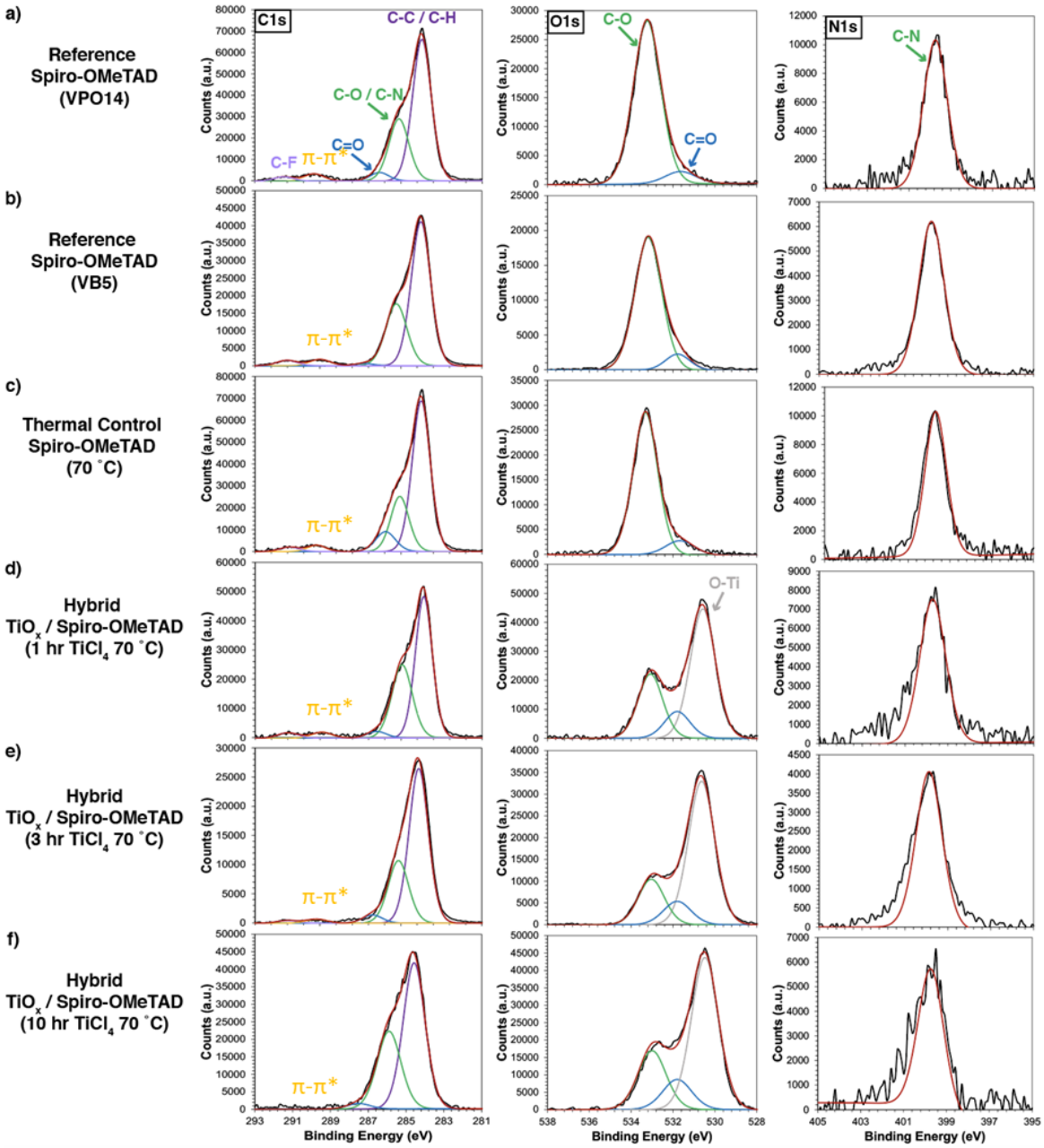

Figure 7 | XPS surface scans of infiltrated spiro-OMeTAD with varying exposure time. (A) Spiro-OMeTAD without VPI. (B) Replica of spiro-OMeTAD without VPI. (C) Thermal control (10 h 70 ˚C simulated VPI without $TiCl_4$). (D) TiOx:spiro-OMeTAD infiltrated with 1 h TiCl4 exposure at 70 ˚C. (E) TiOx:spiro-OMeTAD infiltrated with 3 h TiCl4 exposure at 70 ˚C. (F) TiOx:spiro-OMeTAD infiltrated with 10 h TiCl4 exposure at 70 ˚C.

Planned vs. Actual Activities: This task is considered completed. Infiltration of metal oxides using metal containing precursors by vapor phase infiltration (VPI) and characterization of the resultant physical and chemical structure were done (subtask 2.1 and 2.2). TiOx was detected by X-ray photoelectron

spectroscopy (XPS) and energy-dispersive spectroscopy (EDX), which showed that the Ti content increases with the exposure time during the process. Previous issues to measure a precise infiltration depth were solved. Although direct measurement of the resistivity of the films after infiltration was not possible due to the non-resistive behavior of the SiO_2/TiO_2/spiro-OMeTAD/Au stack, a comparison of the series resistance (Rs) extracted from the J-V scans of complete devices with and without VPI was possible (subtask 2.3). Ultraviolet photoelectron spectroscopy (UPS), UV-VIS absorption, and grazing incidence wide angle X-ray scattering (GIWAXS) were used to evaluate how the properties of the films changed after infiltration.

Explanation of Variance: The infiltration of the metal oxide into the spiro-OMeTAD film was tested, and the properties of hybrid TiOx:spiro-OMeTAD characterized. This task was completed.

c. Task Number and Title: Task 3.0 – Incorporate infiltrated HTLs (hole transport layers) into a solar cell stack

Planned vs. Actual Activities: A maximum PCE of 18.36% and average PCE of 17.63% were achieved by using 5h exposure time of $TiCl_4$., which is close to the milestone 1.1.3, of achieving 18% average efficiency for infiltrated devices. However, milestone 1.4.1 of achieving 20% average efficiency for infiltrated devices was out of reach. TiOx infiltration was found to be detrimental for the initial performance of the perovskite solar cells due to an energetic barrier created at the spiro-OMeTAD|Au interface. The inherent deep valence band of TiO_2 can trap holes, which increases the recombination on the device and lower the V_{OC}. To overcome this problem, VPI can be used to infiltrate spiro-OMeTAD with different metal oxides such as NiOx, whose energy levels are favorable for the hole extraction in a perovskite solar cell. Optimization of the metal precursor used to infiltrate the spiro-OMeTAD layer could lead to devices with higher efficiency, and it will be considered as a follow up project.

Despite lowering the initial performance of the solar cells, TiO_X infiltrated devices have an improved long-term stability compared to the reference. Devices with treated films retain around 80% of their initial efficiency after an operando stability test at 75 °C under AM 1.5 illumination for 60 h, double of the efficiency retained by devices without treated films. This increase in stability is related to TiO_X infiltration hindering the crystallization of the spiro-OMeTAD layer, as evidenced by GIWAXS and XPS measurements. This first demonstration of VPI on a HTL opens a new promising pathway for increasing the stability of perovskite solar cells as well as in other organic electronic devices that rely on these layers.

<u>Milestone 1.3.3 - Perovskite layer preserves optical absorption below 780 nm after deposition of infiltrated layer</u>

We found that the VPI process does not significantly change the optical absorption spectrum. **Figure 8** compares the absorption spectra of samples with varying exposure time of $TiCl_4$. We observe that the region from 400nm to 1000nm is almost unchanged for all the samples. The bandgap of the perovskite layer before and after VPI was calculated using Tauc plot, and it remains constant at 1.53 eV. This proves that VPI is not detrimental for the optical properties of the perovskite layer.

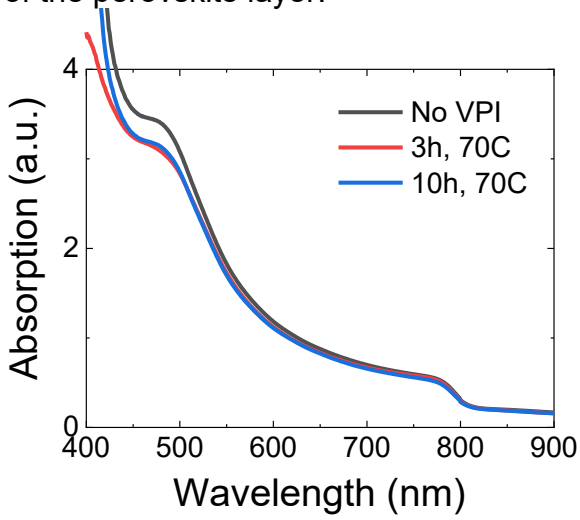

Figure 8 | Transmittance spectra of reference and infiltrated samples (FTO/cTiO2/mpTiO2/PVK/spiro-OMeTAD (varying VPI exposure time of $TiCl_4$)

Milestone 1.1.3 - 18% Average efficiency for infiltrated devices
Milestone 1.4.1 - 20% average efficiency for infiltrated devices

Infiltrated spiro-OMeTAD layers were successfully incorporated in the device stack. The efficiency of devices continuously increased along with the efficiency of the reference devices. Further, introducing a double passivation of the perovskite layer with PEAI (bottom and top interface) was essential to minimize the performance loss induced by the VPI process, but there is still a drop of 50 mV in the Voc, which is responsible of a ~2% PCE loss, as shown in **Figure 9**. This drop in the Voc is not dependent on the exposure time, and it was related to the presence of TiOx in the spiro-OMeTAD layer. Devices that underwent a thermal control process (without $TiCl_4$ exposure) did not show changes in the V_{OC}.
UV-VIS absorption measurements of the spiro-OMeTAD layer show that the bandgap of the material is not modified by TiOx infiltration. However, UPS shows that the valence band of TiOx dominates on the surface of the material. We calculated a work function of -5.06 eV for the untreated films and a work function of -7.1 eV for the infiltrated films, which does not change significantly for $TiCl_4$ exposure times between 3 h and 10 h. Nonetheless, a comparison of the shape of the UPS scans suggests that there is also some signal being obtained from the spiro-OMeTAD on the surface of the infiltrated samples. Moreover, it has also been shown that defects in the structure of TiO_X forms

deep traps that can transport holes in PSCs[40], which can also mitigate the energetic barrier created at the spiro-OMeTAD|Au interface. Therefore, it is possible that holes are being transported by the Spiro-OMeTAD in the hybrid film or by the TiO_X clusters themselves, or by both, but an increased recombination is expected in TiOx infiltrated devices, which explains the drop in the V_{OC}.

To try solving this limitation and reach the 20% average efficiency target using the same reference device, a different metal oxide with better energetics for the hole extraction must be used to infiltrate the spiro-OMeTAD layer. We obtained preliminary results using $VOCl_3$ as the metal precursor in the VPI process. We found that the VO_X infiltration behaves similarly to TiO_X, but the presence of VO_X was even more detrimental for the performance of the solar cells than the TiO_x infiltration, mostly ascribed to a lower Jsc in the VOx-treated films. We hypothesize the decrease in current to be related with the formation of a bigger injection barrier in the HTL interface, which limits further the charge carrier extraction. NiOx is widely used as HTL in perovskite solar cells, for instance, we expect a more favorable energetics when using this material. We are currently developing a protocol to deposit NiO_x via ALD using $Ni(tBuAMD)_2$ as precursor. The process will be the base for the subsequent VPI of the metal oxide into the spiro-OMeTAD layer.

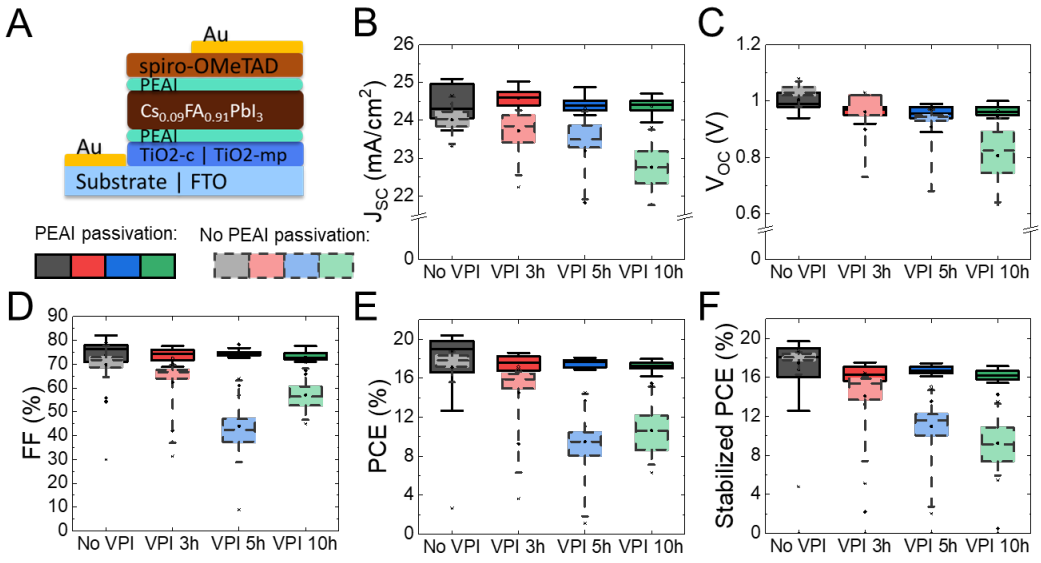

Figure 9 | Electrical characterization of PSCs containing hybrid TiOX:spiro-OMeTAD layers with and without a capping layer of PEAI to protect the bulk of the perovskite layer during the VPI process. A) Device architecture. B) JSC, C) VOC, D)FF and E) PCE obtained from reverse J-V curves. F) Stabilized PCE taken with 1 min of maximum power point tracking (MPPT).

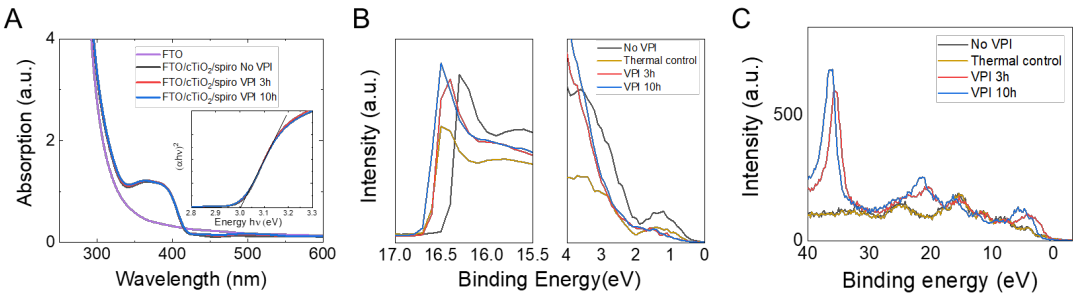

Figure 8 | Optoelectronic properties of the infiltrated spiro-OMeTAD. A) UV-VIS absorption spectra and Tauc plot. B) UPS spectra. (Left) Zoom in on the position of the work function. (Right) Zoom in on the position of the valence band maxima. C) XPS Valence band scan.

Task Number and Title: Task 4.0 – Stakeholder Engagement
Planned vs. Actual Activities: Two solar companies with active research on metal halide perovskites and with expertise on vapor deposition processes have been contacted and agreed to an interview in-person to provide feedback on the technology developed: First Solar, and Swift Solar. Both companies demonstrated interest in a process able to enhance the thermal stability of interface layers. Cost of materials was not identified as a risk for industrial implementation. However, the time required for post-treatment to stabilize the interface was pointed as a potential risk to implementation. The specific choice of spiro-OMeTAD as interlayer to be stabilized was not seen as a risk by First Solar but was pointed out as potentially problematic by Swift Solar. Swift Solar motivated the doubt relating it to the costs involved to perform the transition to a device architecture incorporating spiro-OMeTAD from their current architecture (optimization and collection of new data). Applicability of the technology also to different materials such as PCBM is a plus.

Milestone EOP– <u>T95 500 hours at 85°C and 50% relative humidity in infiltrated devices environment for reference devices</u>

Infiltrated devices have an improved long-term stability compared to the reference as shown in **Figure 9A**. After 4000 h of storage in dark at room temperature, and in a nitrogen environment, the reference devices lost about 16% of the initial efficiency (to an average stabilized PCE of 15%). On the other hand, infiltrated devices only lost about 6% of their initial efficiency (to an average stabilized PCE of 16%). The performance drop is mainly attributed to a decrease in FF and J_{SC}. After 4000 h, the reference devices lost about 10% of FF and 1 mA/cm^2 of J_{SC}.

The effect of VPI on the stability can be seen more clearly when stressing the devices at high temperature and under illumination (**Figure 7B**). We therefore stressed the devices by heating the cells to 85 °C on a hotplate (at open circuit) for 24 h in a nitrogen environment and exposed them to 1 Sun equivalent illumination by a commercial LED lamp. After the stress test, the reference

devices yield a median stabilized PCE that drops to of 1.1%, whereas the TiO_X infiltrated devices provide a stabilized PCE of around 6%. Further stability measurements were carried out by tracking the maximum power point of the devices while keeping constant the temperature of the films (by Peltier pads) at 75 °C under AM1.5 illumination. The MPPT was interrupted every two hours to measure J-V curves under dark and illumination conditions. **Figure 9C** compares the average normalized efficiency obtained in the test. In the first 10 h, all devices suffer a similar decay in the performance, losing around 20% of the original PCE. For longer stress times, infiltrated devices with exposure time between 3 and 10 h reach a plateau in the efficiency, but devices without VPI continue to drop until reaching 40% of the starting efficiency after 60 h.

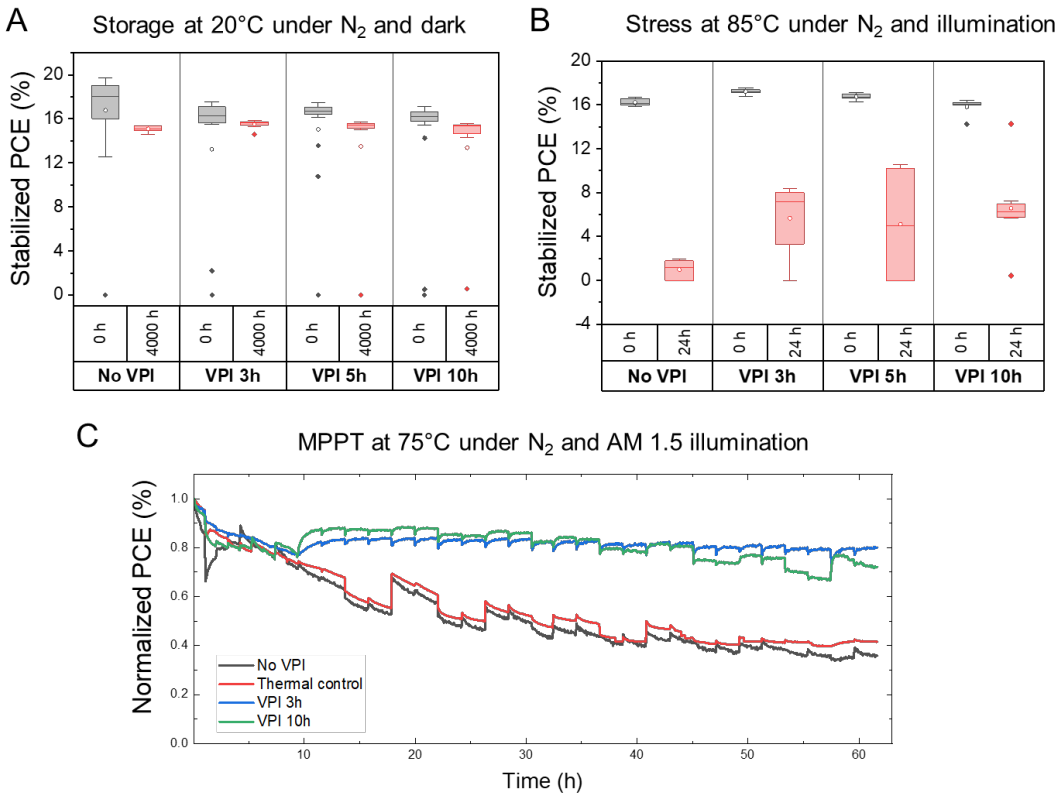

Figure 9 | Stability test under different condition. A) Shelf storage. B) Stress at 85 °C and illumination. C) Operando stability test at 75 °C.

To understand the potential degradation mechanisms that lead to the drop in efficiencies in these PSCs, we conducted UV-vis spectroscopy and x-ray diffraction of the films. UV-VIS absorption spectra of devices taken before and after degradation show that the onset at around 800 nm remains unchanged (**Figure 10A**, 1.54 eV from the Tauc plot), suggesting that, despite changes happening in the layer, the bulk of the perovskite is not affected by the stress test at high temperature and illumination. XRD confirms that the bulk of the perovskite layer is predominantly cubic, and that the intensity of the peaks of

δ-$FAPbI_3$ does not increase, as shown in **Figures 10B**. Therefore, these observations suggest the degradation is likely to happen in a different layer or at an interface.

To investigate if the loss in performances of the solar cells after the stress test was dominated by spiro-OMeTAD crystallization, we measured GIWAXS of the films before and after a thermal treatment at 85 °C for 48 h under illumination. We compared the circular integration of the GIWAXS pattern taken with incident angles (α) from 0.05° to 0.5° of spiro-OMeTAD layers deposited on silicon wafers and monitored the impact of different $TiCl_4$ exposure times. Since the penetration depth of the X-rays varies based on the incident angle, this data enables us to compare the crystallinity at the surface with the bulk of the spiro-OMeTAD layer. The results are presented in **Figure 10C-E**. The surface (α = 0.05°) of the spiro-OMeTAD layer is where we observed the biggest difference between untreated and infiltrated samples. Before thermal stress, the spiro-OMeTAD layers are predominately amorphous. However, the spiro-OMeTAD without VPI treatment shows a small peak located at q = 2.02 $Å^{-1}$, which highlights the presence of an undetermined crystalline phase (phase 1). This peak has a reduced intensity on the 3 h infiltrated sample, and it is absent in the 10 h infiltrated samples. On the other hand, the diffraction in the bulk scan (α = 0.5°) of all the layers is similar and predominantly amorphous. The intensity of the peak attributed to phase 1 decreases in intensity with respect to the surface scan, suggesting that this phase forms preferentially at the surface. Another undetermined crystalline phase (phase 2) is observed in the bulk, which has a predominant peak located at q = 1.79 $Å^{-1}$. We believe there are two different crystal phases present in the film as the peak of phase 2 is broader than the peak observed in phase 1, and no clear relationship between the intensities of these peaks across samples could be found. We could therefore conclude that vapor phase infiltration of TiO_X in spiro-OMeTAD hinders the formation of phase 1.

This trend can be made more evident by studying the devices after stressing the spiro-OMeTAD layers at 85 °C for 48 h under illumination. Untreated spiro-OMeTAD shows increased crystallinity. The intensity of the phase 1 predominant peak increases by five times, and the phase 2 predominant peak is now evident on the surface. Importantly, these peaks are not present on the surfaces of the infiltrated samples. The bulk of all samples shows only minor changes after the stress. Even though TiO_X infiltrated spiro-OMeTAD is predominantly amorphous, peaks with low intensity appear in the GIWAXS pattern after stressing the layers. Indeed, these peaks are also present on the untreated spiro-OMeTAD after stress. However, the presence of these peaks does not have a clear relationship with the intensity of the predominant peaks of phase 1 and 2. This leads us to believe that these peaks belong to a different crystalline structure (phase 3 or more phases) that is formed under thermal stress and illumination on the surface of the layer.

Pure spiro-OMeTAD has been demonstrated to crystallize with a triclinic P-1 space group[41]. However, the simulated pattern does not match the positions of the peaks observed in this study. Identification of each of these crystalline phases is complicated due to the use of additives to improve the electrical properties of spiro-OMeTAD. Li-TFSI, FK-209 Co(III), and tert-butyl pyridine are added to the solution to dope this material, and could interact with spiro-OMeTAD to induce the formation of different, unidentified crystalline phases.

FTIR, XPS, and UPS suggest that TiO_X does not form persistent chemical bonds with the spiro-OMeTAD molecule. Instead, it infiltrates at the molecular level the top 30-40 nm of the spiro-OMeTAD film. As previously discussed, **Figure 7** shows that longer $TiCl_4$ exposure time decreases the intensity of the π-π* satellite peak in the C 1s spectra, which disappears with 10 h $TiCl_4$ exposure, indicating disruption of the spiro-OMeTAD inter-molecular π-π* bonding. We hypothesize that the infiltrated TiO_X plays an important role in hindering the crystallization of the layers by interrupting π-π* stacking between different spiro-OMeTAD molecules.

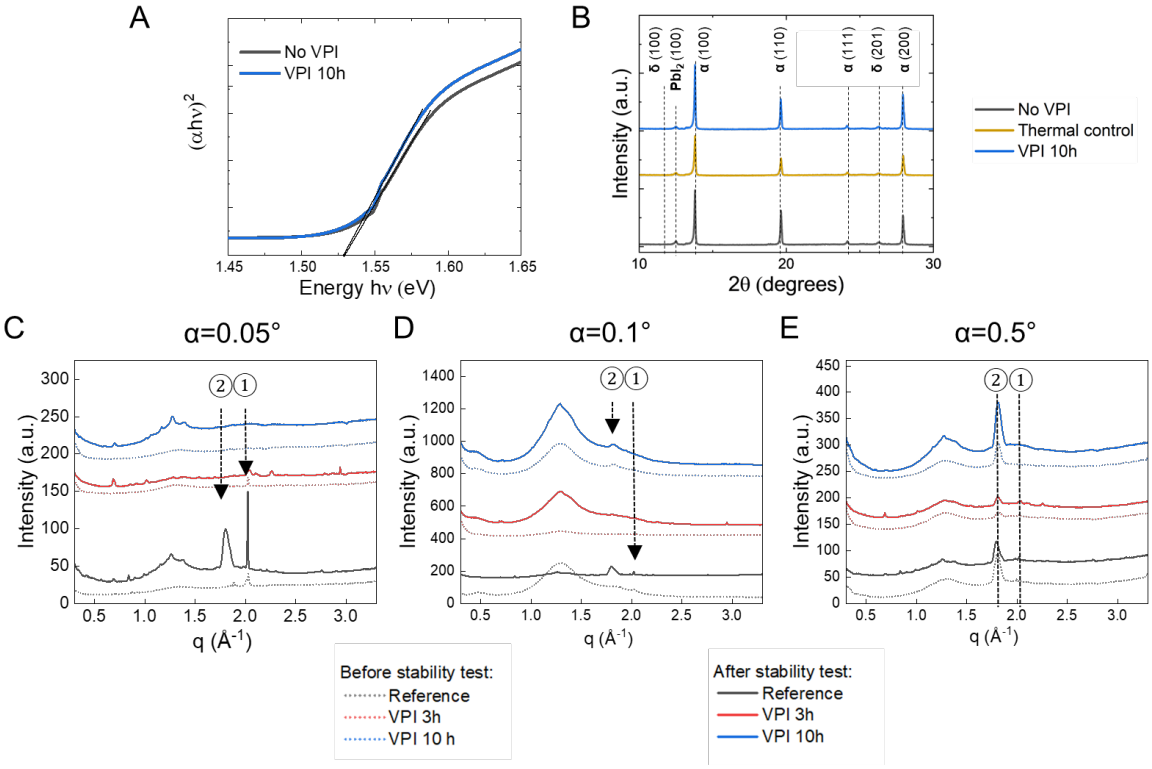

Figure 10 | Characterization of spiro-OMeTAD and devices after degradation. A) UV-VIS absorption spectra. B) XRD patterns. Circular average of GIWAXS patterns of spiro-OMeTAD layer with varying VPI exposure time. C) Incident angle of 0.05° (most surface sensitive). D) Incident angle of 0.1°. E) Incident angle of 0.5° (most bulk sensitive).

Explanation of Variance: Although the detrimental effect of VPI on the initial performance of the devices was minimized. TiO_X infiltration causes a drop of 50mV in the V_{OC} of the solar cells, which limits the performance. To obtain higher efficiencies, a different metal oxide is needed. We believe NiO_X infiltration can provide better energetics and avoid the introduction of non-radiative recombination centers, but the process to infiltrate perovskite solar cells with NiO_X is still under development. On the other hand, VPI showed promising results in the stability test. TiOx infiltrated devices are able to retain double of the PCE of the reference devices after an operando stress at 75 °C under nitrogen environment for 60h. However, reaching the target of T95 after 500h at 85 °C was not possible. Better understanding of the degradation pathways of spiro-OMeTAD at high temperature and at the other solar cell interfaces is needed to further improve the stability of perovskite solar cells containing this layer.

8. **Significant Accomplishments and Conclusions**: This work demonstrates the use of VPI to form hybrid TiO_X:spiro-OMeTAD layers in PSC devices. TiOx infiltrates the top 30-40 nm of the spiro-OMeTAD layer while the remaining bulk is unchanged. Chemical bonding between TiO_X and spiro-OMeTAD is not detected from FTIR or XPS. Further, UV-VIS and XRD show that VPI does not affect the other layers in the complete PSC. However, TiO_X infiltration decreases the V_{OC} of the devices, reducing the initial stabilized PCE by approximately 1.5%. This decrease in the voltage is likely related to an energetic barrier that TiO_X infiltration creates at the surface of the spiro-OMeTAD. On the other hand, TiO_X infiltration increases considerably the long-term stability of devices. Treated films retain around 80% of their initial efficiency after an operando stability test at 75 °C under AM 1.5 illumination for 60h. This increase in stability is related to TiO_X infiltration hindering the crystallization of the spiro-OMeTAD layer, as evidenced by GIWAXS and XPS measurements.

9. **Path Forward:** This first demonstration of VPI on a HTL opens a new promising pathway for increasing the stability of perovskite solar cells as well as in other organic electronic devices that rely on these layers. Further work is needed to achieve higher efficiencies and stability at elevated temperatures and more materials will be needed to explore this avenue.

10. **Inventions, Patents, Publications, and Other Results:**
    a. **Provisional patent application:**

Application No.:	63/400,102
Title:	VAPOR PHASE INFILTRATION AS A TOOL TO IMPROVE THERMAL STABILITY OF ORGANIC LAYERS IN PEROVSKITE SOLAR CELLS
Inventors:	Juan-Pablo Correa-Baena et al.
Applicants:	Georgia Tech Research Corporation
Filing Date:	August 23, 2022
Country:	United States
MCC Reference:	10034-202PV1
GT Reference:	9034

b. Peer reviewed publication:

Castro-Méndez, A. F., Wooding, J. P., Fairach, S., Perini, C. A. R., McGuiness, E. K., J., Vagott, J. N., Li, R., Kim, S., Brahmatewari, V., Dentice, N., Losego, M. D. & Correa-Baena, J. P. **Vapor Phase Infiltration Improves Thermal Stability of Organic Layers in Perovskite Solar Cells**. *ACS Energy Letters. 2023, 8, 1, 844–852*

11. References:

(1) Song, Z.; McElvany, C. L.; Phillips, A. B.; Celik, I.; Krantz, P. W.; Watthage, S. C.; Liyanage, G. K.; Apul, D.; Heben, M. J. A Technoeconomic Analysis of Perovskite Solar Module Manufacturing with Low-Cost Materials and Techniques. *Energy Environ Sci* **2017**, *10* (6), 1297–1305. https://doi.org/10.1039/C7EE00757D.

(2) Kojima, A.; Teshima, K.; Shirai, Y.; Miyasaka, T. Organometal Halide Perovskites as Visible-Light Sensitizers for Photovoltaic Cells. *J Am Chem Soc* **2009**, *131* (17), 6050–6051. https://doi.org/10.1021/JA809598R/SUPPL_FILE/JA809598R_SI_001.PDF.

(3) Yoo, J. J.; Seo, G.; Chua, M. R.; Park, T. G.; Lu, Y.; Rotermund, F.; Kim, Y. K.; Moon, C. S.; Jeon, N. J.; Correa-Baena, J. P.; Bulović, V.; Shin, S. S.; Bawendi, M. G.; Seo, J. Efficient Perovskite Solar Cells via Improved Carrier Management. *Nature 2021 590:7847* **2021**, *590* (7847), 587–593. https://doi.org/10.1038/s41586-021-03285-w.

(4) Min, H.; Lee, D. Y.; Kim, J.; Kim, G.; Lee, K. S.; Kim, J.; Paik, M. J.; Kim, Y. K.; Kim, K. S.; Kim, M. G.; Shin, T. J.; Il Seok, S. Perovskite Solar Cells with Atomically Coherent Interlayers on SnO2 Electrodes. *Nature 2021 598:7881* **2021**, *598* (7881), 444–450. https://doi.org/10.1038/s41586-021-03964-8.

(5) Song, Z.; Abate, A.; Watthage, S. C.; Liyanage, G. K.; Phillips, A. B.; Steiner, U.; Graetzel, M.; Heben, M. J. Perovskite Solar Cell Stability in Humid Air: Partially Reversible Phase Transitions in the PbI2-CH3NH3I-H2O System. *Adv Energy Mater* **2016**. https://doi.org/10.1002/aenm.201600846.

(6) Turren-Cruz, S. H.; Hagfeldt, A.; Saliba, M. Methylammonium-Free, High-Performance, and Stable Perovskite Solar Cells on a Planar Architecture. *Science (1979)* **2018**, *362* (6413), 449–453. https://doi.org/10.1126/SCIENCE.AAT3583/SUPPL_FILE/AAT3583-TURREN-CRUZ-SM.PDF.

(7) An, Y.; Andrea, C.; Perini, R.; Hidalgo, J.; Castro-Mé Ndez, A. S.-F.; Vagott, J. N.; Li, R.; Saidi, W. A.; Wang, S.; Li, X.; Correa-Baena, J.-P. P.; Perini, C. A. R.; Hidalgo, J.; Castro-Méndez, A. F.; Vagott, J. N.; Li, R.; Saidi, W. A.; Wang, S.; Li, X.; Correa-Baena, J.-P. P. Identifying High-Performance and Durable Methylammonium-Free Lead Halide Perovskites via High-Throughput Synthesis and Characterization. *Energy Environ Sci* **2021**, *14* (12), 6638–6654. https://doi.org/10.1039/D1EE02691G.

(8) Jones, D. (Mac); An, Y.; Hidalgo, J.; Evans, C.; Vagott, J. N.; Correa-Baena, J.-P. P. Polymers and Interfacial Modifiers for Durable Perovskite Solar Cells: A Review. *J Mater Chem C Mater* **2021**, *9* (37), 12509–12522. https://doi.org/10.1039/D1TC01243F.

(9) Leijtens, T.; Eperon, G. E.; Pathak, S.; Abate, A.; Lee, M. M.; Snaith, H. J. Overcoming Ultraviolet Light Instability of Sensitized TiO2 with Meso-Superstructured Organometal Tri-Halide Perovskite Solar Cells. *Nat Commun* **2013**. https://doi.org/10.1038/ncomms3885.

(10) Meng, L.; You, J.; Yang, Y. Addressing the Stability Issue of Perovskite Solar Cells for Commercial Applications. *Nature Communications 2018 9:1* **2018**, *9* (1), 1–4. https://doi.org/10.1038/s41467-018-07255-1.

(11) Wang, R.; Mujahid, M.; Duan, Y.; Wang, Z. K.; Xue, J.; Yang, Y. A Review of Perovskites Solar Cell Stability. *Adv Funct Mater* **2019**, *29* (47), 1808843. https://doi.org/10.1002/ADFM.201808843.

(12) Barranco, A.; Lopez-Santos, M. C.; Idigoras, J.; Aparicio, F. J.; Obrero-Perez, J.; Lopez-Flores, V.; Contreras-Bernal, L.; Rico, V.; Ferrer, J.; Espinos, J. P.; Borras, A.; Anta, J. A.; Sanchez-Valencia, J. R. Enhanced Stability of Perovskite Solar Cells Incorporating Dopant-Free Crystalline Spiro-OMeTAD Layers by Vacuum Sublimation. *Adv Energy Mater* **2020**, *10* (2), 1901524. https://doi.org/10.1002/AENM.201901524.

(13) Kasparavicius, E.; Franckevičius, M.; Malinauskiene, V.; Genevičius, K.; Getautis, V.; Malinauskas, T. Oxidized Spiro-OMeTAD: Investigation of Stability in Contact with Various Perovskite

Compositions. *ACS Appl Energy Mater* **2021**, *4* (12), 13696–13705. https://doi.org/10.1021/ACSAEM.1C02375/ASSET/IMAGES/LARGE/AE1C02375_0007.JPEG.

(14) Wang, S.; Yuan, W.; Meng, Y. S. Spectrum-Dependent Spiro-OMeTAD Oxidization Mechanism in Perovskite Solar Cells. *ACS Appl Mater Interfaces* **2015**, *7* (44), 24791–24798. https://doi.org/10.1021/ACSAMI.5B07703/ASSET/IMAGES/AM-2015-07703F_M010.GIF.

(15) Domanski, K.; Correa-Baena, J. P.; Mine, N.; Nazeeruddin, M. K.; Abate, A.; Saliba, M.; Tress, W.; Hagfeldt, A.; Grätzel, M. Not All That Glitters Is Gold: Metal-Migration-Induced Degradation in Perovskite Solar Cells. *ACS Nano* **2016**, *10* (6), 6306–6314. https://doi.org/10.1021/ACSNANO.6B02613/ASSET/IMAGES/LARGE/NN-2016-026139_0006.JPEG.

(16) Domanski, K.; Correa-Baena, J. P.; Mine, N.; Nazeeruddin, M. K.; Abate, A.; Saliba, M.; Tress, W.; Hagfeldt, A.; Grätzel, M. Not All That Glitters Is Gold: Metal-Migration-Induced Degradation in Perovskite Solar Cells. *ACS Nano* **2016**, *10* (6), 6306–6314. https://doi.org/10.1021/ACSNANO.6B02613/ASSET/IMAGES/LARGE/NN-2016-026139_0006.JPEG.

(17) Meng, Q.; Chen, Y.; Xiao, Y. Y.; Sun, J.; Zhang, X.; Han, C. B.; Gao, H.; Zhang, Y.; Yan, H. Effect of Temperature on the Performance of Perovskite Solar Cells. *Journal of Materials Science: Materials in Electronics* **2021**, *32* (10), 12784–12792. https://doi.org/10.1007/S10854-020-03029-Y/FIGURES/6.

(18) Sheikh, A. D.; Munir, R.; Haque, M. A.; Bera, A.; Hu, W.; Shaikh, P.; Amassian, A.; Wu, T. Effects of High Temperature and Thermal Cycling on the Performance of Perovskite Solar Cells: Acceleration of Charge Recombination and Deterioration of Charge Extraction. *ACS Appl Mater Interfaces* **2017**, *9* (40), 35018–35029. https://doi.org/10.1021/ACSAMI.7B11250/ASSET/IMAGES/LARGE/AM-2017-11250N_0008.JPEG.

(19) Tumen-Ulzii, G.; Qin, C.; Matsushima, T.; Leyden, M. R.; Balijipalli, U.; Klotz, D.; Adachi, C. Understanding the Degradation of Spiro-OMeTAD-Based Perovskite Solar Cells at High Temperature. *Solar RRL* **2020**, *4* (10), 2000305. https://doi.org/10.1002/SOLR.202000305.

(20) Sheikh, A. D.; Munir, R.; Haque, M. A.; Bera, A.; Hu, W.; Shaikh, P.; Amassian, A.; Wu, T. Effects of High Temperature and Thermal Cycling on the Performance of Perovskite Solar Cells: Acceleration of Charge Recombination and Deterioration of Charge Extraction. *ACS Appl Mater Interfaces* **2017**, *9* (40), 35018–35029. https://doi.org/10.1021/ACSAMI.7B11250/ASSET/IMAGES/LARGE/AM-2017-11250N_0008.JPEG.

(21) Sun, S.; Buonassisi, T.; Correa-Baena, J. P. State-of-the-Art Electron-Selective Contacts in Perovskite Solar Cells. *Adv Mater Interfaces* **2018**, *5* (22), 1–9. https://doi.org/10.1002/admi.201800408.

(22) You, J.; Meng, L.; Song, T. Bin; Guo, T. F.; Chang, W. H.; Hong, Z.; Chen, H.; Zhou, H.; Chen, Q.; Liu, Y.; De Marco, N.; Yang, Y. Improved Air Stability of Perovskite Solar Cells via Solution-Processed Metal Oxide Transport Layers. *Nat Nanotechnol* **2016**, *11* (1), 75–81. https://doi.org/10.1038/nnano.2015.230.

(23) Rolston, N.; Printz, A. D.; Tracy, J. M.; Weerasinghe, H. C.; Vak, D.; Haur, L. J.; Priyadarshi, A.; Mathews, N.; Slotcavage, D. J.; McGehee, M. D.; Kalan, R. E.; Zielinski, K.; Grimm, R. L.; Tsai, H.; Nie, W.; Mohite, A. D.; Gholipour, S.; Saliba, M.; Grätzel, M.; Dauskardt, R. H. Effect of Cation Composition on the Mechanical Stability of Perovskite Solar Cells. *Adv Energy Mater* **2018**, *8* (9), 1–7. https://doi.org/10.1002/aenm.201702116.

(24) Rolston, N.; Bush, K. A.; Printz, A. D.; Gold-Parker, A.; Ding, Y.; Toney, M. F.; McGehee, M. D.; Dauskardt, R. H. Engineering Stress in Perovskite Solar Cells to Improve Stability. *Adv Energy Mater* **2018**, *8* (29), 1–7. https://doi.org/10.1002/aenm.201802139.

(25) Rolston, N.; Bush, K. A.; Printz, A. D.; Gold-Parker, A.; Ding, Y.; Toney, M. F.; McGehee, M. D.; Dauskardt, R. H. Engineering Stress in Perovskite Solar Cells to Improve Stability. *Adv Energy Mater* **2018**, *8* (29), 1802139. https://doi.org/10.1002/aenm.201802139.

(26) Seo, S.; Shin, S.; Kim, E.; Jeong, S.; Park, N. G.; Shin, H. Amorphous TiO2Coatings Stabilize Perovskite Solar Cells. *ACS Energy Lett* **2021**, *6* (9), 3332–3341. https://doi.org/10.1021/ACSENERGYLETT.1C01446/ASSET/IMAGES/LARGE/NZ1C01446_0005.JPEG.

(27) Deng, K.; Li, L.; Deng, K.; Li, L. Advances in the Application of Atomic Layer Deposition for Organometal Halide Perovskite Solar Cells. *Adv Mater Interfaces* **2016**, *3* (21), 1600505. https://doi.org/10.1002/ADMI.201600505.

(28) Seo, S.; Jeong, S.; Park, H.; Shin, H.; Park, N. G. Atomic Layer Deposition for Efficient and Stable Perovskite Solar Cells. *Chemical Communications* **2019**, *55* (17), 2403–2416. https://doi.org/10.1039/C8CC09578G.

(29) Choi, E. Y.; Kim, J.; Lim, S.; Han, E.; Ho-Baillie, A. W. Y.; Park, N. Enhancing Stability for Organic-Inorganic Perovskite Solar Cells by Atomic Layer Deposited Al2O3 Encapsulation. *Solar Energy Materials and Solar Cells* **2018**, *188*, 37–45. https://doi.org/10.1016/J.SOLMAT.2018.08.016.

(30) Rajbhandari, P. P.; Dhakal, T. P. Low Temperature ALD Growth Optimization of ZnO, TiO2, and Al2O3 to Be Used as a Buffer Layer in Perovskite Solar Cells. *Journal of Vacuum Science & Technology A: Vacuum, Surfaces, and Films* **2020**, *38* (3), 032406. https://doi.org/10.1116/1.5139247.

(31) Zardetto, V.; Williams, B. L.; Perrotta, A.; Di Giacomo, F.; Verheijen, M. A.; Andriessen, R.; Kessels, W. M. M.; Creatore, M. Atomic Layer Deposition for Perovskite Solar Cells: Research Status, Opportunities and Challenges. *Sustain Energy Fuels* **2017**, *1* (1), 30–55. https://doi.org/10.1039/C6SE00076B.

(32) Brinkmann, K. O.; Gahlmann, T.; Riedl, T. Atomic Layer Deposition of Functional Layers in Planar Perovskite Solar Cells. *Solar RRL* **2020**, *4* (1), 1900332. https://doi.org/10.1002/SOLR.201900332.

(33) Correa Baena, J. P.; Steier, L.; Tress, W.; Saliba, M.; Neutzner, S.; Matsui, T.; Giordano, F.; Jacobsson, T. J.; Srimath Kandada, A. R.; Zakeeruddin, S. M.; Petrozza, A.; Abate, A.; Nazeeruddin, M. K.; Grätzel, M.; Hagfeldt, A. Highly Efficient Planar Perovskite Solar Cells through Band Alignment Engineering. *Energy Environ Sci* **2015**, *8* (10), 2928–2934. https://doi.org/10.1039/c5ee02608c.

(34) Waldman, R. Z.; Mandia, D. J.; Yanguas-Gil, A.; Martinson, A. B. F.; Elam, J. W.; Darling, S. B. The Chemical Physics of Sequential Infiltration Synthesis—A Thermodynamic and Kinetic Perspective. *J Chem Phys* **2019**, *151* (19), 190901. https://doi.org/10.1063/1.5128108.

(35) Leng, C. Z.; Losego, M. D. Vapor Phase Infiltration (VPI) for Transforming Polymers into Organic–Inorganic Hybrid Materials: A Critical Review of Current Progress and Future Challenges. *Mater Horiz* **2017**, *4* (5), 747–771. https://doi.org/10.1039/C7MH00196G.

(36) Leng, C. Z.; Losego, M. D. Vapor Phase Infiltration (VPI) for Transforming Polymers into Organic-Inorganic Hybrid Materials: A Critical Review of Current Progress and Future Challenges. *Mater Horiz* **2017**, *4* (5), 747–771. https://doi.org/10.1039/c7mh00196g.

(37) McGuinness, E. K.; Zhang, F.; Ma, Y.; Lively, R. P.; Losego, M. D. Vapor Phase Infiltration of Metal Oxides into Nanoporous Polymers for Organic Solvent Separation Membranes. *Chemistry of Materials* **2019**, *31* (15), 5509–5518. https://doi.org/10.1021/ACS.CHEMMATER.9B01141/ASSET/IMAGES/LARGE/CM-2019-01141H_0004.JPEG.

(38) Mcguinness, E. K.; Leng, C. Z.; Losego, M. D. Increased Chemical Stability of Vapor-Phase Infiltrated AlOx-Poly(Methyl Methacrylate) Hybrid Materials. *ACS Appl Polym Mater* **2020**, *2* (3), 1335–1344. https://doi.org/10.1021/ACSAPM.9B01207/ASSET/IMAGES/LARGE/AP9B01207_0009.JPEG.

(39) Bamford, J. T.; Smith, R. A.; Leng, C. Z.; Gutekunst, W. R.; Losego, M. D. Measuring the Glass Transition Temperature of Vapor-Phase-Infiltrated AlO x-PS- r-PHEMA Organic-Inorganic Hybrid Thin-Film Materials. *Macromolecules* **2021**, *54* (14), 6790–6798. https://doi.org/10.1021/ACS.MACROMOL.1C00691/ASSET/IMAGES/LARGE/MA1C00691_0007.JPEG.

(40) Seo, S.; Shin, S.; Kim, E.; Jeong, S.; Park, N. G.; Shin, H. Amorphous TiO2Coatings Stabilize Perovskite Solar Cells. *ACS Energy Lett* **2021**, *6* (9), 3332–3341. https://doi.org/10.1021/ACSENERGYLETT.1C01446/ASSET/IMAGES/LARGE/NZ1C01446_0005.JPEG.

(41) Shi, D.; Qin, X.; Li, Y.; He, Y.; Zhong, C.; Pan, J.; Dong, H.; Xu, W.; Li, T.; Hu, W.; Brédas, J. L.; Bakr, O. M. Spiro-OMeTAD Single Crystals: Remarkably Enhanced Charge-Carrier Transport via Mesoscale Ordering. *Sci Adv* **2016**, *2* (4). https://doi.org/10.1126/SCIADV.1501491/SUPPL_FILE/1501491_SM.PDF.